IN FLIGHT AERODYNAMIC EXPERIMENT FOR THE UNMANNED SPACE VEHICLE FTB-1

G.C. Rufolo, M. Marini, P. Roncioni, S. Borrelli
CIRA, Italian Aerospace Research Centre
Via Maiorise - 81043 Capua
Italy

OVERVIEW

Aim of this paper is to show preliminary results of the in-flight aerodynamic experiment carried out within the frame of USV project, the first space experimental vehicle funded by the Italian National Aerospace Research Program (PRO.R.A.). The Unmanned Space Vehicle FTB-1 (Flying Test Bed 1) is a multi-mission, re-usable vehicle designed, developed and built at CIRA[1]. The first mission DTFT (Dropped Transonic Flight Test) was performed on February 24th, 2007 from the base of Arbatax in Sardinia (Italy) and it was aimed at experimenting the transonic flight of a re-entry vehicle. The core of the experiment has been based on the gathering of static pressure measurements over the vehicle surface during the flight. By means of CFD computations the most *interesting* regions of the vehicle in terms of fluid dynamic complexity have been identified, and 304 static pressure probes have been located in these regions. Each sensor is constituted by a pressure tap, a pneumatic line (i.e. a flexible tube), and a piezoelectric transducer that converts the pressure signal into an electrical one. The overall collecting of pressure ports is obtained by means of 6 ESP (Electronically Scanned Pressure) modules. All the data collected in flight have to be corrected for pressure lag (due to pneumatic lines) and correlated with the quantities determining the state of the vehicle and with the measurements of global aerodynamic coefficients obtained by inertial measurements. Moreover, some selected flight conditions occurred during the DTFT mission of the FTB-1 vehicle have been numerically rebuilt, the attention being focused on the surface pressure distributions to be compared with in-flight pressure measurements. After the execution of CFD simulations, results have to be critically analyzed and compared to flight data in order to find out indications about the *quality* of the entire CFD methodology (grid generation, turbulence and transition modelling, etc.).

1. VEHICLE AND MISSION DESCRIPTION

The USV FTB-1 vehicle can be classified as a winged body, see FIG. 1. The main body of FTB-1 has an overall length of 8000 mm, from the nose apex (without considering the air data boom) up to the base plate. The front fuselage ends with a pointed nose constituted by a quasi-conical shape closed by a 1-cm radius hemisphere. Downstream of the pointed nose, the windside part of the forebody geometry rapidly changes from a quasi-circular to a rounded-square shape. The mid-fuselage is characterized by a quasi-constant section while the afterbody ends with a boat-tailed truncated base. The wing of the FTB-1 vehicle has a double delta shape with a main 45 deg sweepback leading edge and a strake with a 76 deg sweepback leading edge. The trailing edge has a sweepforward angle of 6 deg. To improve lateral stability, the FTB-1 wing has a dihedral angle of 5 deg with respect to the wing reference plane. Overall wing span is 3562 mm, while the strake root chord is 2820 mm. An elevon with both functions of elevator and aileron is mounted on the FTB-1 wing.

For directional stability and control a V-Tail solution has been adopted: the two vertical tails have a dihedral angle of 40 deg, a sweepback angle of 45 deg and a span of 800 mm. A pair of full-span movable rudders is also implemented for directional control.

FIG. 1. FTB-1 and gondola suspended from the launch machine before flight

Moreover, in order to augment directional stability characteristics of the vehicle and to reduce possibilities of Dutch-roll occurrence a pair of full symmetric ventral fins has been also added. Ventral fins, without movable surfaces, are characterized by a 55 deg sweepback angle, a root chord of 800 mm with a taper ratio of 0.455, and a span of 418 mm. Their design has been conceived in order to have the highest effectiveness with the lowest impact on structure.

The first USV FTB-1 mission has been aimed at experimenting the transonic flight of a re-entry vehicle. In the frame of a step-by-step approach, the USV FTB-1 will perform additional missions, each of them with an increasing maximum Mach number (up to Mach 2), thus simulating the final portion of a typical re-entry trajectory. The USV FTB-1 vehicle is basically composed by a Flying Test Bed and a Carrier based on a stratospheric balloon[1]. During the missions the balloon carries the FTB-1 up to the desired altitude (around 20 km for the first mission) and then, after having established a cruise horizontal trajectory, releases it from the gondola. At this

moment the FTB-1 vehicle starts its own flight following the designed trajectory.

The main target of the aerodynamic experiment has been to provide a database of in-flight measurements of global (forces, moments) and local (static pressures) aerodynamic parameters useful to support and improve the CFD tools employed for the vehicle's design. In particular, the objective of the experiment performed during this first FTB-1 mission has been the evaluation of the effect of a Mach number sweep, at nearly constant angle-of-attack, on the longitudinal global aerodynamic coefficients and, through comparison between the upper and lower part of the descent, the effect of Reynolds number (the large altitude variation causes a wide range of Reynolds number during the flight).

The mission aerodynamic requirements of this first DTFT mission are reported in the table below.

	Profile	Range	Notes
Mach	sweep	0.7 → M_{max} → 0.7	acceleration/ deceleration
Reynolds	f (M, z)	$10^6 \div 10^7$	
α (AoA)	const.	≥ 4 deg	
β (AoS)	const.	0 deg	longitudinal symmetric flight

TAB. 1. DTFT mission aerodynamic requirements

Flight recorded data in the temporal frame useful for the aerodynamic experiment are described in Sec. 5.

2. THE AERODYNAMIC PREDICTION MODEL

In order to properly describe the aerodynamic characteristics of the USV FTB-1 vehicle it has been necessary to develop a suitable Aerodynamic Prediction Model (APM), i.e. a mathematical representation of the physics of the problem.

Hereinafter, a brief description of this model together with an overview of the source of data used for its development is given with the aim at clarifying the need for in-flight aerodynamic experimentation. In the case of a winged body as the USV FTB-1 vehicle, the aerodynamic properties to be characterized are the six global aerodynamic coefficients (C_L, C_D, C_Y : lift, drag and side forces; C_l, C_m, C_n : rolling, pitching and yawing moments), the hinge moments (C^i_H) of the control devices (elevons, rudders) and the surface pressure distribution (p_w). Starting from the knowledge of the real phenomenology and basing on previous experience it has been possible to define the functional structure of the APM: for each of the six aerodynamic coefficients a dependence from a suitable subset of independent variables $\{M, \mathrm{Re}, \alpha, \beta, \delta^r_E, \delta^l_E, \delta^r, p, q, r, \dot{\alpha}\}$ has been assumed.

A classical build-up approach[2] has been used for the description of the global aerodynamic coefficients, where each coefficient is expressed as a linear summation over a certain number of contributions, each of them dependent by a small number of parameters. In general, each aerodynamic coefficient C_i has the following structure:

$$\mathrm{C_i}\left(M, \mathrm{Re}, \alpha, \beta, \delta^r_E, \delta^l_E, \delta_R, \dot{\alpha}, p, q, r\right) = \\ = \mathrm{C_i^{BL}} + \Delta\mathrm{C_i^{\beta}} + \Delta\mathrm{C_i^{\delta_e}} + \Delta\mathrm{C_i^{\delta_r}} + \Delta\mathrm{C_i^{\dot{\alpha}}} + \Delta\mathrm{C_i^{p}} + \Delta\mathrm{C_i^{q}} + \Delta\mathrm{C_i^{r}} \quad (1)$$

The term $C_i^{BL}(M, \mathrm{Re}, \alpha)$ represents the baseline contribution to the global coefficient C_i at zero-sideslip in clean configuration (with no-deflection of control surfaces) and with no dynamic effects. The other terms represent the delta coefficient related to the variable indicated as apex. Once the APM is defined, it is necessary to gather a sufficient amount of data in order to explicit the functional dependencies of each piece of the model. Data sources considered are: wind tunnel, CFD and engineering methods. In particular, for the development of the USV FTB-1 Aero-Data-Base (ADB) the primary source of data has been represented by the test campaigns carried out within the CIRA PT-1 transonic wind tunnel[3] and the Transonic Wind-tunnel Göttingen (TWG) of DNW consortium[4],[5].

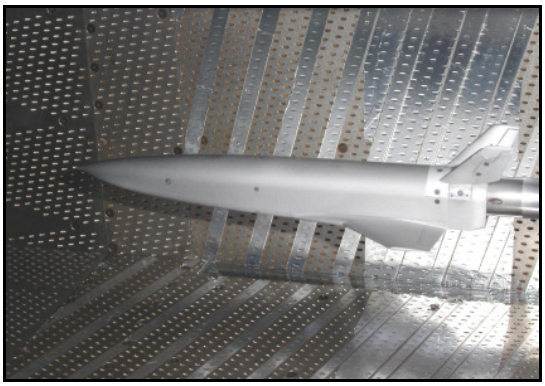

FIG. 2. CIRA PT-1 facility test chamber with the USV FTB-1 scaled (1:30) model

In FIG. 2 a picture of the 1:30 USV FTB-1 scaled model installed within the porous test chamber of the CIRA PT-1 transonic wind tunnel is shown. In FIG. 3 a Schlieren colour image taken at TWG is also reported, showing the complex shock waves and vortex pattern around the vehicle at supersonic Mach number and non-zero sideslip flow condition.

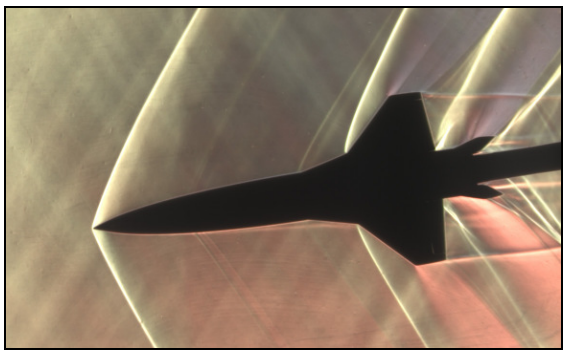

FIG. 3 Schlieren image at M=1.2, α=10 deg, β=8 deg

CFD data have been primarily used to cross-check wind tunnel data and to fill measurements gaps, e.g. the effects of base drag, Reynolds number and model support system interference[6]. In addition, simplified numerical methods like Eulerian CFD, Vortex Lattice Method (VLM), Panel Method (PM) and DATCOM have been used to fill existing gaps in wind tunnel data for M<0.5, to provide a rapid estimation of configuration changes occurring during the design process, and mainly to provide dynamic stability derivatives[7],[8],[9]. It has been shown that Eulerian CFD is quite useful to provide a suitable preliminary estimation of aerodynamic coefficients in transonic regime, where it is well known that approximate methods (VLM, PM, DATCOM) begin to fail[7].

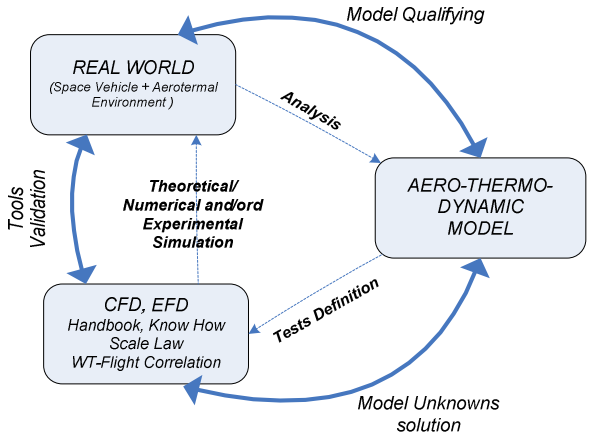

FIG. 4. The APM graphical representation

By following the logical process reported in FIG. 4, wind tunnel test campaigns have been designed taking into account the hypotheses made in the APM in order to optimize test matrices.

The data collected during the experimental test campaigns do not allow for a complete characterization of the FTB-1 aerodynamics with respect to all the interesting parameters: a typical example is the effect of Reynolds number. Therefore, experimental data (the base of the ADB) must be properly corrected by means of scaling laws describing Reynolds number effects, and these laws have been obtained with the help of CFD simulations. Moreover, the necessity to correct wind tunnel measurements derives also by other factors such as the presence of a model support (i.e. the sting) and the impossibility to include the base contribution in the total drag measurement. The general expression used for the calculation of the *extrapolated-to-flight* aerodynamic coefficients (left hand side terms) is the following:

$$\begin{aligned} C_i^{Flight} &= C_i^{WT} + \Delta C_i^{Sting} + \Delta C_i^{\mathrm{Re}\ press},\ i = \{\mathrm{L, Y, l, m, n}\} \\ C_D^{Flight} &= C_D^{WT} + \Delta C_D^{Base} + \Delta C_D^{Sting} \\ &+ \Delta C_D^{\mathrm{Re}\ fric} + \Delta C_D^{\mathrm{Re}\ press} \end{aligned} \qquad (2)$$

where the in-flight values correspond to the Reynolds number encountered along the nominal trajectory, the first terms on the right hand side are the wind tunnel measured coefficients and the remaining terms are the CFD-based corrections: base drag, sting interference, variation of friction drag with Reynolds number, effect of Reynolds number over the forebody pressure drag. The sting effect on the vehicle's forebody is obviously neglected in supersonic regime.

To account for Reynolds number variation effects, the general approach is to correct each global aerodynamic coefficient with a function of Reynolds number, i.e.

$$\begin{aligned} C_i(Re_{FL}) &= C_i(Re_{WT}) + f(Re_{WT}, Re_{FL}) = \\ &= C_i(Re_{WT}) + g(Re_{FL}) - g(Re_{WT}) \end{aligned} \qquad (3)$$

As a general rule, second order polynomial interpolation has been found versus the logarithm of Reynolds number[6], i.e.

$$g(\mathrm{Re}) = a\log_{10}^2(\mathrm{Re}) + b\log_{10}(\mathrm{Re}) + c \qquad (4)$$

Concerning the base drag contribution it has to be said that the existing empirical correlations for base drag are strongly problem-dependent an therefore CFD seems to be the most reliable way of correcting wind tunnel data, although it is well known that a lot of difficulties exist in the right prediction of large re-circulating base flow regions. FIG. 5 reports a typical CFD-based function describing the base drag correction (ΔC_D^{Base}).

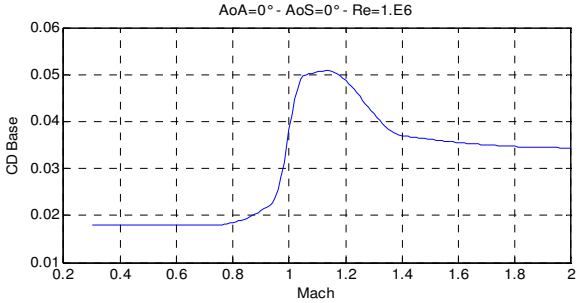

FIG. 5. The ΔC_D^{Base} correction vs. Mach number

Beside the information regarding the global aerodynamic coefficients, a detailed CFD analysis has been also useful in order to obtain a deeper understanding of the entire vehicle's aerodynamics. In FIG. 6 an example of the flow features predicted by CFD computations is reported. It is possible to note the formation of the leading vortex, typical of delta-wing configuration, and its interaction with both the wing-tip and the strake vortex. This kind of analysis strongly helps the correct understanding of the wind tunnel measurements.

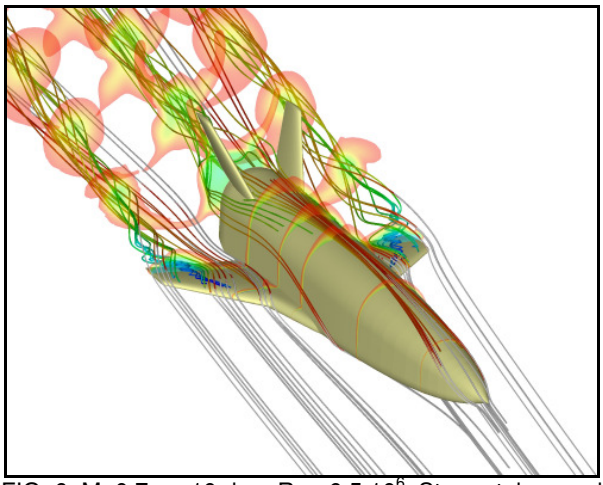

FIG. 6. M=0.7, α=10 deg, Re= $6.5\cdot10^6$. Streamtubes and iso-contours of total pressure

As it will be shown in the following, one of the main objectives of the in-flight pressure measurements is to validate and eventually improve the CFD tools necessary to provide wind tunnel data corrections.

Once wind tunnel data have been suitably corrected, it is possible to build the set of functional contributions describing the aerodynamic coefficients and consequently the ADB as well. In FIG. 7 the ADB function for the lift coefficient at M=0.94, clean configuration and zero sideslip is plotted in function of the angle of attack, together with the sources of data available (PT-1 wind tunnel, DNW/TWG wind tunnel, CFD).

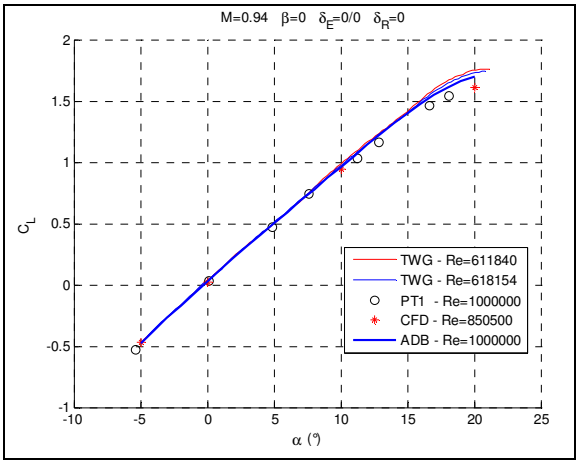

FIG. 7. C_L vs. α (M=0.94, β=0°, clean configuration).

Even though the Aerodynamic Prediction Model is aimed at being the best possible by exploiting the available tools and know-how, it remains however a representation of the actual phenomenology, and therefore it is characterized by errors. To assess the APM output data it is then necessary to estimate the entity of such errors, by associating to the *nominal values* provided by the APM the related *uncertainty margins***.** The *uncertainty model* associated to the present APM is characterized by a proper functional structure, and by a certain number of basic parameters[10].

Without going into the details, it can be said that each of the terms of the uncertainty model is obtained as a sum of different contributions due to the different parts of the APM (WT, CFD)[11]. To such traceable error sources it has to be added the uncertainty due to the *ignorance*, i.e. the incapacity of predicting any unexpected phenomenology not foreseen by the APM during the flight. As an example, FIG. 8 shows the uncertainties envelope included in the USV FTB-1 Aero-Data-Base for the term $C_{m\alpha}$.

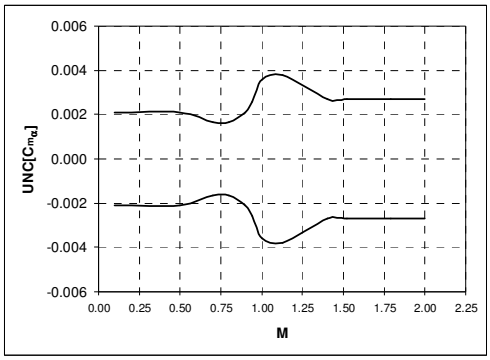

FIG. 8. $C_{m\alpha}$ parameter uncertainty vs. Mach number

3. AERODYNAMIC EXPERIMENT: LOGIC AND EXPECTATIONS

The aerodynamic characterization of a space vehicle in the transonic part of the re-entry trajectory is made difficult by the strong variability of the aerodynamic coefficients (typical of this regime) due to the flow field nonlinearities, these latter ones induced by the formation of shock waves on the body surface and by the detachment of vortex structures. Also the need for peculiar design solutions, like for instance the truncated base and the double V-Tail, makes critical the accurate prediction of aerodynamic parameters. Moreover, the extended range of altitude of the mission envelope causes a large variation of Reynolds number and, as a consequence, the necessity of an extrapolation-to-flight methodology whose reliability is related to the validation of CFD tools.

In this frame it is very important to compare the outputs of the Aerodynamic Prediction Model to the in-flight measurements. In particular, the main benefits obtainable by gathering in-flight data may be recognized in the following items:

1. *Validation of predictive capabilities of Computational Fluid Dynamics (CFD) codes for a complex configuration in flight conditions.*
2. *Validation of the suitability of the Wind-Tunnel Test methodology.*
3. *Validation and tuning of the methodology for the extrapolation to flight conditions of the experimental measurements.*
4. *Reduction of the uncertainty margins associated with the pre-flight prediction of the aerodynamic coefficients.*

Within the frame of the USV project, the main goal of the in-flight experimentation relies on the *evaluation of predictive capability and in its improvement finalized to risk reduction*. Thus, after the comparison between aerodynamic prediction and in-flight measurements it could be possible to reduce the uncertainty on global aerodynamic coefficients and to improve the set-up of the APM with referring, in particular, to the extrapolation-to-flight procedure. Moreover, the gathered data constitute a database to be used for validation and improvement of the numerical models for the simulation of flight conditions (e.g. turbulence modelling).

The comparison pre/post-flight is performed by acquiring, during the flight, both the global aerodynamic coefficients (forces and moments) and the local parameters (static pressures). In particular, the former ones are functional to the evaluation of the uncertainty margins and then to the goodness of the APM, while the latter ones allow the detailed evaluation of the quality of the *tools* used for prediction.

Pre-flight predictions obtained by using the Aerodynamic Prediction Model, in terms of global aerodynamic coefficients and stability derivatives, will be compared to in-flight measured data (provided with their own uncertainty bands). In particular, the flight conditions in terms of freestream quantities and control surfaces (elevons, rudders) deflections along the entire flown trajectory will be used as inputs for the APM, and the outputs of the model will be compared to the in-flight measured data.

Some selected flight conditions occurred during the DTFT mission of the FTB-1 vehicle will be numerically rebuilt, the attention being focused to the surface pressure distributions to be correlated with in-flight pressure measurements. As a rule of thumb, numerical simulations will be aimed at reproducing the most relevant fluid dynamic phenomena characterizing the USV FTB-1 aerodynamics. After the execution of these CFD simulations, results will be analysed and compared to flight data and, if necessary, an assessment of the entire CFD methodology (grid generation, turbulence and transition modelling, etc.) will be carried out.

All the information deriving from the aerodynamic experiment will be finally used to improve the existing APM. This improvement will be pursued on different levels. First of all, an assessment and, if possible, a reduction of the uncertainty margins will be achieved by comparing them with the difference between pre-flight predictions and flight data (in terms of global aerodynamic coefficients). Then the APM structure will be critically analyzed with respect to the flight data in order to optimize the functional dependencies and/or the number of parameters which the aerodynamic prediction model depends upon. Finally, the analysis of the local measurements of pressure at different altitude (high and low branch of the trajectory) and the comparison with the CFD data and the skin-friction lines visualizations performed in the DNW/TWG facility will allow for a deeper understanding of the Reynolds number effects with the aim at improving the extrapolation-to-flight procedure.

4. EXPERIMENTAL SET-UP

In the previous section it has been shown that both global and local aerodynamic measurements are needed to accomplish the objectives of the USV experimentation plan. The aerodynamic forces and moments are derived starting from measurements of vehicle's accelerations and attitude during flight. This activity is being carried out by Flight Mechanics (FM) and Guidance, Navigation and Control (GN&C) teams, and no further details will be given hereinafter.

In the following the set-up of the experiment for the measurement of surface pressure during flight is described. The analysis of surface pressure distribution obtained by means of CFD simulations for different flight conditions (M=0.7, 0.94, 1.05; α=0,10 deg) has allowed to identify the most interesting regions in terms of maximum gradients and maximum variations with respect to Mach number and vehicle attitude. In particular, the attention has been focused on the following regions: the NOSE, with the aim at studying a flush mounted air data system; the WING, the lifting surface with the maximum pressure variation and presence of shock waves in transonic regime; the MID and REAR FUSELAGE, characterised by large pressure variations in non symmetric flight conditions and strong interference caused by the upper and lower V-Tails; the BASE, with an extended re-circulating flow region, thus causing many difficulties for numerical prediction. For each of this region a set of locations for static pressure probes has been identified. Number and position of pressure probes have been selected accordingly to these criteria: phenomenon reproducibility, structural compatibility, technological feasibility. In FIG. 9 the locations of pressure probes superimposed to the pressure coefficient field at M=1.05 and α=10 deg are reported. An overall number of 304 locations has been selected for pressure measurements.

Being the aim of the experiment to *capture* quasi-steady phenomena, a classical architecture has been adopted, i.e. the pressure sensor is constituted by a pressure tap connected by means of a pneumatic line to an electronic transducer.

The pressure tap is constituted by an orifice over the vehicle's surface to which a short metallic gauge tube is glued. The internal diameter of the orifice is 0.8 mm. This value has been selected as a good compromise between measurement accuracy, the larger is the hole the lower is the accuracy, and pneumatic line dynamic response, the larger is the hole the lower is the signal damping.

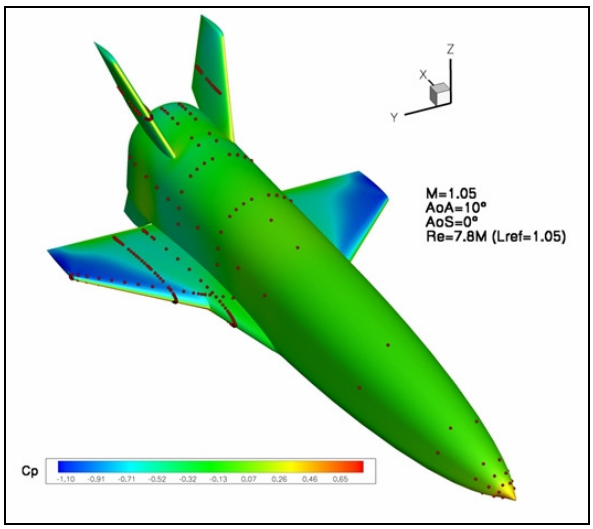

FIG. 9. Pressure coefficient iso-contours with pressure taps positions

Polyurethane tubes are connected to the metallic ones by means of helicoils and convey the pressure signal to the transducers. In FIG. 10 an internal view of the composite wing leading edge with a detail of the pressure ports installation along a wing section is depicted; moreover, it is clearly visible the complex routing of the pneumatic lines that need to be as short as possible and with the minimum number of bending. As a matter of fact a theoretical-numerical analysis has been carried out in order to understand which are the optimal tube diameter and the maximum allowable length ensuring a frequency filtering characteristic higher than 1Hz.

FIG. 10. Internal view of the wing leading edge with the pressure taps metallic inserts and pneumatic tubing

The 304 pressure lines are collected by means of 6 Electronically Scanned Pressure (ESP) miniaturised piezoelectric modules produced by SCANIVALVE CORPORATION®. In particular, models ZOC22B/32Px–5Psid-Valveless and ZOC33/64Px–5Psid-Valveless have been used, that are respectively capable of collecting 32 and 64 pressure ports. These sensors measure differential pressure, therefore a dedicated channel acquires the reference pressure (from the flight-boom). The ESP modules are characterized by a full scale of 5psid and a nominal accuracy of 0.1%FS. In order to minimize the transducers error due to temperature

variation, each module is encapsulated in a Thermal Control Unit (TCU) which is also water proof in order to guarantee ESP reusability. In FIG. 11 an internal view of the TCU with the ZOC and the tubing connecting the transducers ports to the quick connector is shown, while in FIG. 12 the layout of the ESP modules is represented.

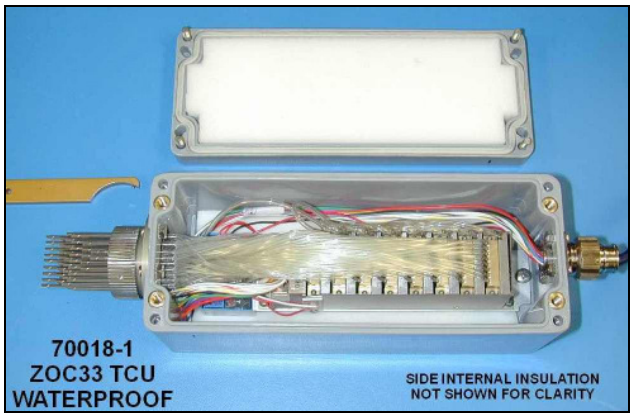

FIG. 11. Internal view of the thermal control unit with the ESP and pneumatic connections

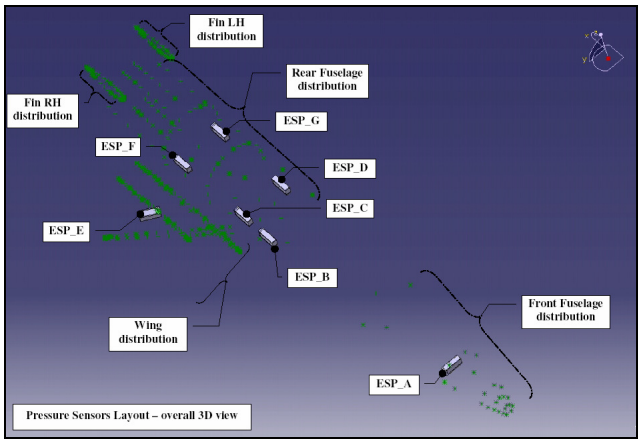

FIG. 12. Pressure Scanners Layout

whose time shift is due to the dynamic response of the sensors pneumatic lines, a software tool has been properly developed, although it has not yet been applied because it has to be validated against experimental tests (still on-going). Furthermore, additional tests are planned for pressure scanners inside a climatic chamber to characterise the effect of temperature variation during the flight on the sensor accuracy. In the meantime, these corrections are not yet considered in the results presented in this paper.

FIG. 13 describes the distribution of quantities defining the flight conditions (M, AoA, AoS, P_s, δ_E, δ_R) in function of time elapsed from the beginning of the temporal window useful for the experimental activities. The air data have been acquired by means of a Pitot-static flight boom positioned on the nose (see FIG. 1), while the angle of attack and sideslip are measured with vains. As it can be noted, the angle of attack, in the controlled phase, remained nearly constant at a value of 7.5 deg. A quick decrease can be observed at about t=31 sec, when the elevon efficiency has rapidly decreased in transonic regime, and the control system has required a small time to compensate it. The angle of sideslip has been kept around zero for the whole trajectory.

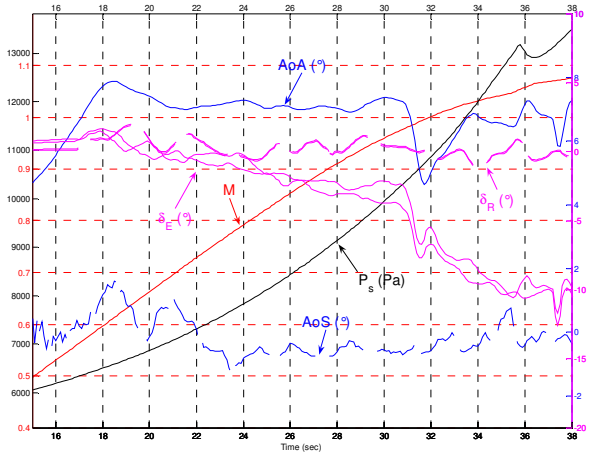

FIG. 13. Temporal distribution of flight parameters

5. EXPERIMENTAL RESULTS

Hereinafter some results of the local pressure measurements experiment are shown. More details can be found in Sec. 7, where the comparison between experimental and CFD data are shown.

The global aerodynamic forces and moments are not presented in this paper, since at the time of writing the post-processing of such flight data is still on-going.

It has to be said that in order to make experimental data exploitable it is necessary to accurately know as a function of time along the *as flown* trajectory, the entire set of flight conditions: altitude, air speed, aircraft attitude, control surfaces deflections. Starting from these information, it is then possible to rebuild, by means of three dimensional Navier-Stokes calculations, the real flight conditions and, as a consequence, to validate the used CFD modelling (computational grids, turbulence model, laminar-turbulent transition, etc.).

Moreover, in order to properly synchronize the pressure measurements with the flight point knowledge,

In FIG. 14, FIG. 15 and FIG. 16 temporal histories of pressure coefficient for a selected number of pressure taps is reported. It has to be remarked that the ESP measures the differential between the local static pressure and the asymptotic one. In order to obtain the pressure coefficient this value has been divided by the dynamic pressure calculated with measured asymptotic Mach number and pressure. In particular, in FIG. 14 the temporal histories of C_p for four sensors of the wing section W3 (Y=1000 mm from symmetry plane), indicated with arrows of the same colours of the plot lines, are reported. It can be noted the expansion peak (tap B-04) over the leeside and the compression one (tap B-16) over the windside, both located immediately downstream of the leading edge. It is also interesting to see how these peaks varies at t=31 sec when the angle of attack suddenly decreases from 7.5 deg to about 5 deg, with a subsequent movement of the stagnation point on the wing leading edge (and a reduction of the lift coefficient).

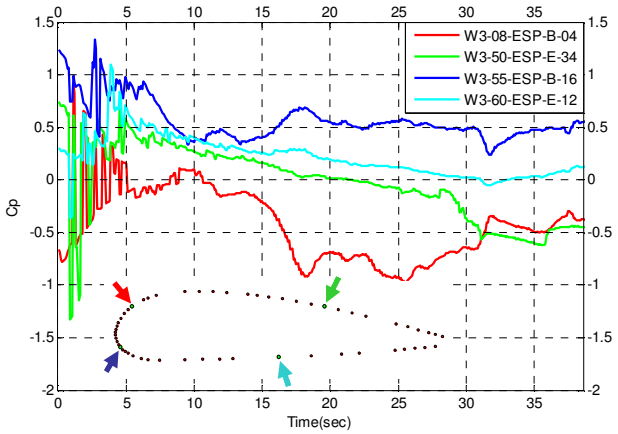

FIG. 14. Pressure coefficient versus time for selected taps along a wing profile (Y=1000 mm from symmetry plane)

In FIG. 15, the distribution of pressure coefficient versus time for a line of sensors distributed over the front fuselage (section FF4, 1200 mm from the nose apex) is reported. The readings of these sensors are useful for the qualification of a Flush Mounted Air Data system (FADS) to be used for future missions, and provide useful information for a cross-check verification of the in-flight angles of attack and sideslip. Also in this case, it can be noted the variation of C_p corresponding to the sharp variation of angle of attack at t=31 sec.

Base plate measurements of pressure coefficient are reported in FIG. 16. As expected the values of the three sensors in function of time are quite similar, and again a sharp variation is observed at t=31 sec with an increase of the base contribution to the total aerodynamic drag.

As a general rule, it has to be observed that for the initial portion of the acquisition window (up to t=10 sec) the scattering of the readings is very high. This is due to the fact that the transducers error (a constant value equal to the 0.1% of the full scale) becomes more and more significant when the pressure is very low.

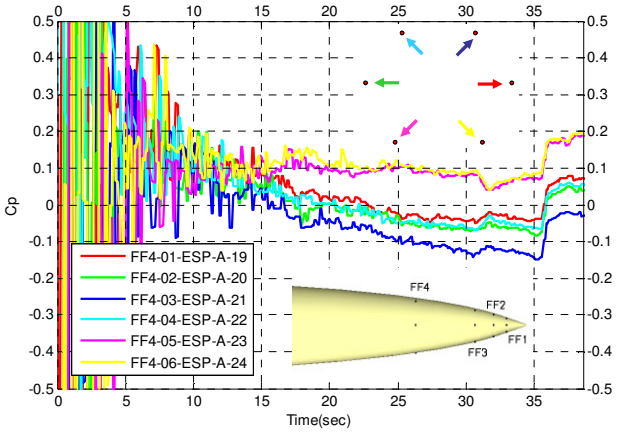

FIG. 15. Pressure coefficient versus time for pressure taps along FF4 section (X=1200 mm from nose apex)

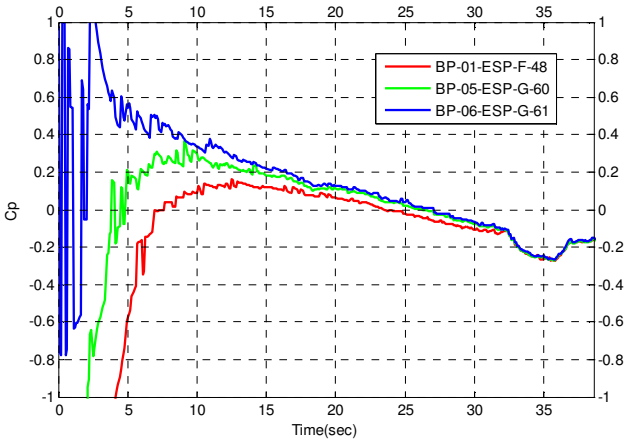

FIG. 16. Pressure coefficient versus time for pressure taps over the base plate

6. CFD NUMERICAL REBUILDING

As already stated, in order to achieve the experimentation goals described in Sec. 3 it is necessary to numerically rebuild some selected flight conditions. The final objective of the first DTFT mission post-flight activity is to carry out full three-dimensional Navier-Stokes simulations with laminar-to-turbulent transition. In this preliminary phase only Eulerian calculations have been performed, and computed results are reported in the following.

6.1. Trajectory Points Selection

As a rule of thumb, numerical simulations should be aimed at reproducing the most relevant fluid dynamic phenomena characterizing the USV FTB-1 vehicle aerodynamics. Looking at the flown flight trajectory, five flight conditions have been selected and reported in TAB. 2. In FIG. 17, the angle of attack measured along the trajectory versus time is reported; with red circles the flight conditions selected to be rebuilt are indicated.

Time	AoA	AoS	Mach	$Rey_{L=1.05}$	δ_{ER}	δ_{EL}	δ_{RR}	δ_{RL}
[sec]	[deg]	[deg]	[-]	[-]	[deg]	[deg]	[deg]	[deg]
21.5	7.00	0.39	0.703	1854452	-0.77	-0.37	1.27	1.22
28.8	6.95	-0.45	0.901	3161851	-2.71	-3.09	0.88	0.80
30.8	7.24	-0.70	0.940	3549761	-2.43	-4.11	0.38	0.31
31.3	6.03	-0.37	0.951	3665483	-5.56	-6.78	0.06	-0.01
36.6	6.87	-0.20	1.052	4899732	-9.82	-10.21	-0.55	-0.61

TAB. 2. Trajectory points selected for CFD simulations

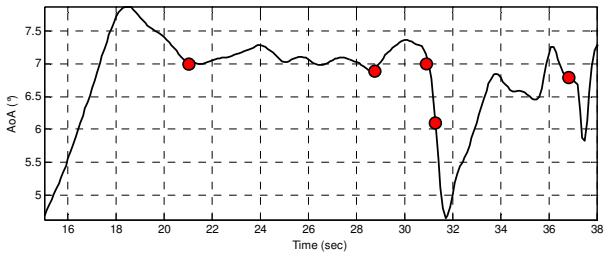

FIG. 17. Angle of attack versus time: red circles indicate flight points selected for CFD simulations

6.2. CFD Code: H3NS

The numerical code used to carry out the aerodynamic analysis of the USV FTB-1 vehicle is the CIRA code H3NS, developed and validated by the Laboratory of

Aerothermodynamics and Space Propulsion[12], that solves the Reynolds Average Navier-Stokes equations in a density-based finite volume approach with a cell centred Flux Difference Splitting second order ENO-like upwind scheme for the convective terms. Both equilibrium and non-equilibrium thermo-chemistry is available and a compressible two-equation k-ε turbulence modelling can be used for eddy viscosity calculation.

The code has been run either on the CIRA Super Computer NEC TX-7 (scalar-parallel supercomputer with 20 1500MHz processors Itanium2, 40 GB of central memory and a total peak power of 120 GFLOPS), either on personal computers (3.20 GHz Intel Pentium D processor, 2GB of RAM).

6.3. Computational Grids

The multi-block structured grids have been generated by using the commercial software package ICEMCFD-HEXA (version 5.1).

The grid around half vehicle with a symmetry laying on the centre-plane XZ is composed by four main O-grids (see FIG. 18 and FIG. 19). After a local block decomposition that fixes the topology around the fuselage and the wing, a first O-grid has been generated for the fuse-wing part, then other two O-grids for the vertical tail and ventral and finally the last one for the base.

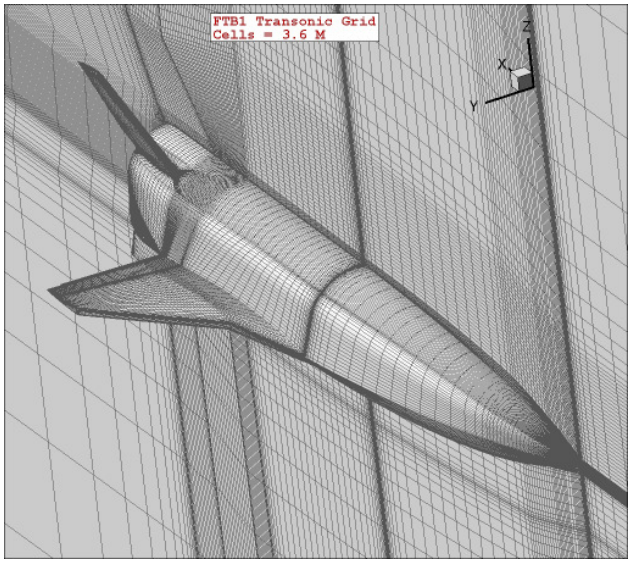

FIG. 18. FTB-1 Transonic Grid. 3.6 million of cells

The external boundary of the half-body grid has been built as a Cartesian block with far-field surfaces located at about ten body lengths far from the body.

Since the scope of the numerical simulations is to rebuild some relevant points of the flown trajectory, a grid for each of these points, characterized by a different control device (see TAB. 2) deflection, has been generated. The gaps both along chord-wise and span-wise directions between the elevon (right part of the vehicle only) and the wing/fuse part have not been considered. The resulting wedge topology has been meshed by using collapsed faces at wall, properly treated by the CFD code H3NS.

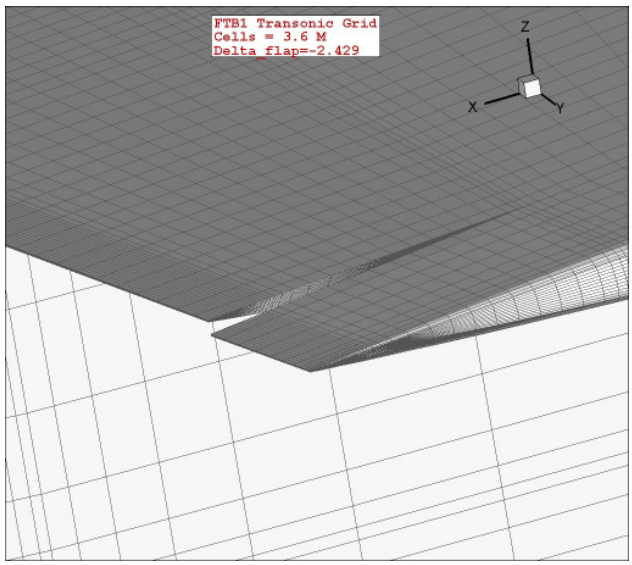

FIG. 19. FTB-1 Transonic Grid. Mesh around the deflected elevon

The Eulerian version of the grid has about 3.6 million of cells and 146 blocks. It has been built with three grid levels in order to perform a grid sensitivity analysis. After this analysis a less demanding grid (3 million of cells) has been used for the remaining CFD simulations.

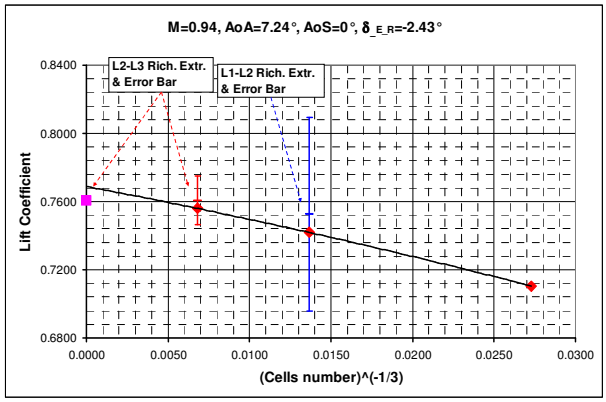

FIG. 20. Grid sensitivity. Lift coefficient

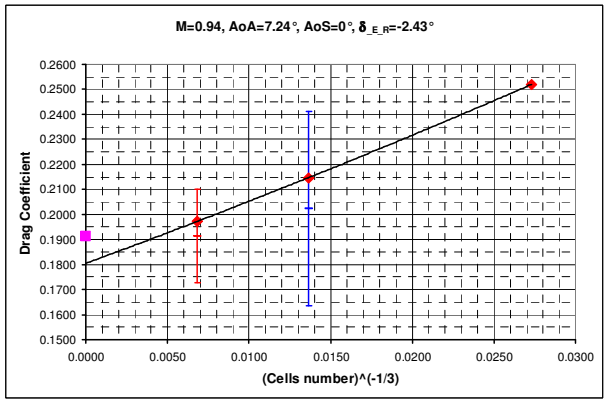

FIG. 21. Grid sensitivity. Drag coefficient

The grid sensitivity analysis has been carried out at M=0.94, α=7.24 deg, β=0 deg and δ_E^R =-2.43 deg by using three levels of the structured multiblock grid. The number of cells of the finest level (L_3) is respectively 8 and 64 times the one of the medium (L_2) and the coarse (L_1) levels.

From FIG. 20 and FIG. 21 it is possible to observe as the trend of global aerodynamic coefficients versus the inverse of the cubic root of the number of cells (representative of the degree of grid resolution) is in the asymptotic range of convergence. In this way it is possible to use the Richardson extrapolation formulas to obtain higher order values for the global coefficients (value at virtually zero cell dimension!) and a contribution to the whole uncertainty levels due to the grid dependence of global aerodynamic coefficients. The error bars of the L_2-L_3 and L_1-L_2 Richardson extrapolated values, as obtained with the above said theory, are reported in the grid convergence plots (FIG. 20 and FIG. 21). It is interesting to note as the L_2-L_3 error bar is fully contained within the L_1-L_2 one. In addition, as a good convergence indicator, we can note as the L_1-L_2 extrapolated value is contained within the L_2-L_3 error-bar.

As a conclusion of the global grid sensitivity analysis, we can see that, for the particular case considered, there is an under-estimation for C_L (-1.87%) and an over-estimation for C_D (9.80%). It must be said that, as a general rule for such complex geometry, the maximum number of cells used for the present simulations was selected in accordance with an acceptable convergence CPU time estimation.

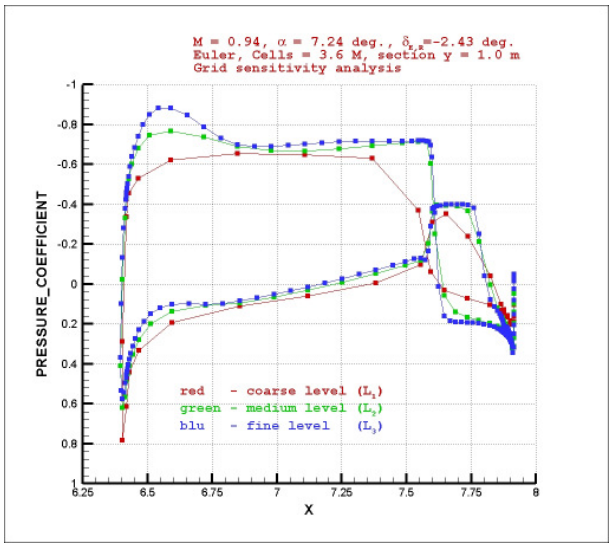

FIG. 22. Grid sensitivity. Pressure coefficient at y=1.0 m

A local grid convergence can be observed also from FIG. 22, where the chord-wise pressure coefficient distribution is reported, for the analysed flight condition, at the y=1.0 m wing section. The asymptotic range of convergence has been reached for nearly all the positions.

6.4. Numerical Results

In this section an analysis of the preliminary Eulerian results is given. As said previously, five points of the flight trajectory have been selected for the CFD rebuilding and subsequent comparison with in-flight local pressure measurements.

It must be pointed out that CFD computations (see TAB. 2) have been performed in the hypothesis of no sideslip angle (β=0 deg) on the half-body grids, and assuming as elevon deflection the one of the right wing device (δ_E^R), where the pressure sensor are located, and no rudder deflection (δ_R^R=0 deg).

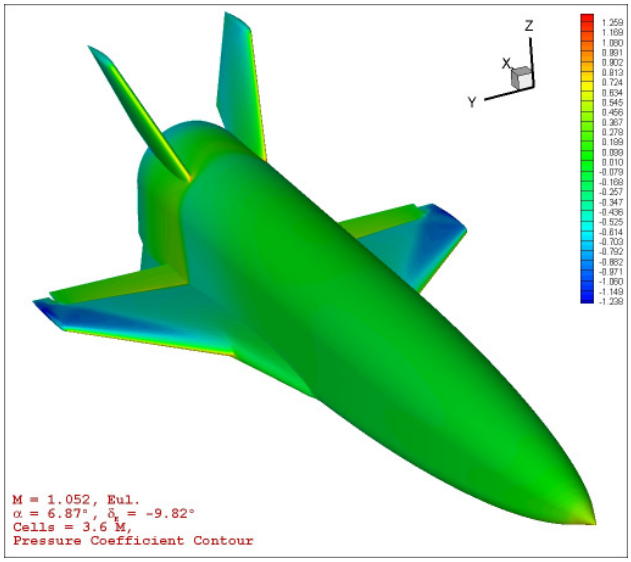

FIG. 23. Pressure coefficient contours (M=1.052, α=6.87 deg, δ_E^R =-9.82 deg)

As an example of predicted flow features in flight conditions, a strong shock wave can be observed laying on the fuselage, just in front of the V-tails, and along the elevon hinge line for the M=1.052 case (see FIG. 23).

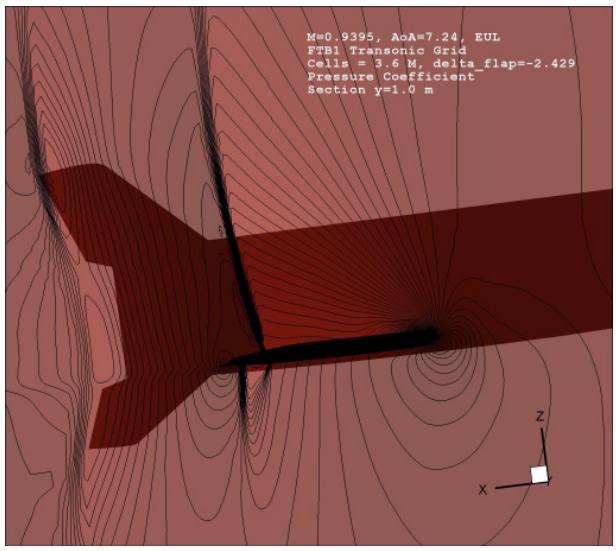

FIG. 24. Pressure coefficient contours at section y=1.0 m

In particular, from FIG. 24 a clear phenomenology can be observed for the M=0.94 flight condition around the elevon hinge-line: a strong compression wave on the leeside and an expansion and a subsequent recompression (over the elevon) on the windside. This

CFD predicted behaviour is confirmed by the experimental Schlieren image of FIG. 25, taken during the DNW/TWG test campaign at the same Mach number, α=5 deg and with the model clean configuration.

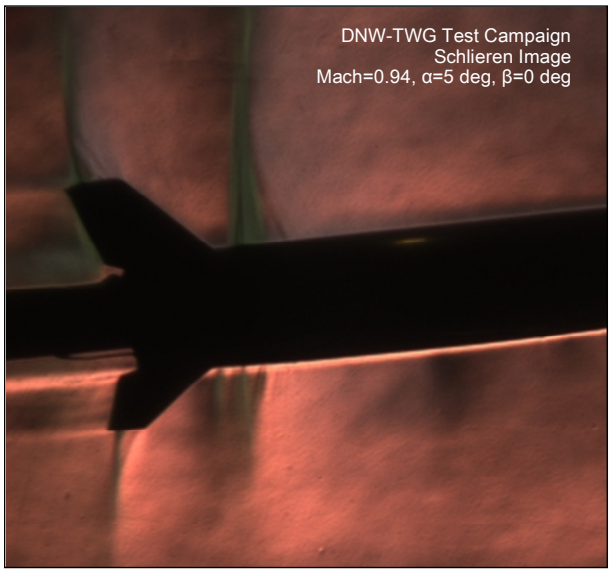

FIG. 25. DNW-TWG Schlieren image (M=0.94, α=5 deg)

It can be concluded that the comparison between CFD and Wind Tunnel results has shown a good agreement from the qualitative point of view, in the sense that predicted and experimentally observed flow features are very similar.

7. CFD VERSUS FLIGHT DATA COMPARISON

In this section the comparison between the preliminary CFD Eulerian results (see TAB. 2) and the in-flight pressure measurements is reported. The comparisons between predicted and in-flight measured global aerodynamic forces and moments are not presented in this paper, since at the time of writing the post-processing of such flight data is still on-going.

A lot of data have been analyzed and compared. All the numerical pressure distributions along the sections containing the in-flight pressure taps have been extracted. However, for lack of space only a selected number of results, and related comparisons, have been shown hereinafter. The comparisons between predicted and in-flight measured pressure coefficients at the wing section W3 (y=1.0 m from the vehicle's symmetry plane) are reported from FIG. 26 to FIG. 29.

A similar trend can be observed from FIG. 26 and FIG. 27, respectively for M=0.901 and M=0.940 at the wing section W3. For both cases the expansion and subsequent recompression on the windside can be clearly seen in both numerical predictions and in-flight measurements. The leeside shock wave is located more upstream for the M=0.901 case with respect to the M=0.94 condition, and this is more evident due to the better definition of discontinuities given by Eulerian simulations. However, both the predicted expansion and compression peaks just downstream of the stagnation point at wing leading edge compare very well with the in-flight measurements. Moreover, in both flight conditions Eulerian computations, as expected, do not predict the deterioration of pressure field on leeside (i.e. a recompression shock), due to the large separated area existing at these relatively high angles of attack, that starts for this wing section at about mid-chord position.

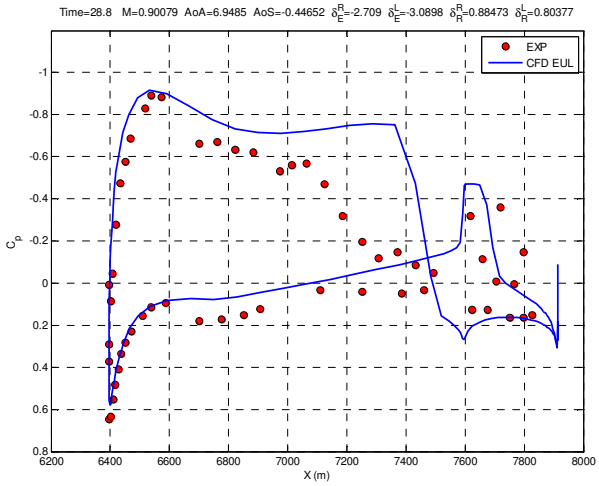

FIG. 26. Pressure coefficient at wing section y=1.0 m (M=0.901, α=6.95 deg, δ_E^R =-2.71 deg)

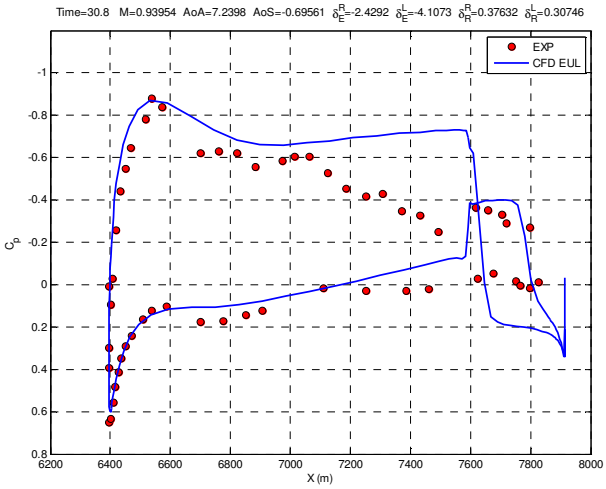

FIG. 27. Pressure coefficient at wing section y=1.0 m (M=0.94, α=7.24 deg, δ_E^R =-2.43 deg)

The case M=0.951 (see FIG. 28) is characterized by a greater elevon deflection with respect to the previous cases, and the CFD prediction shows a larger expansion and the positioning of the windside shock wave exactly at the wing trailing edge. This is not in agreement with the experimental finding where the shock wave seems to be still over the elevon. Again, this can be explained by the absence of viscous effects in the CFD simulations. The predicted levels of pressure coefficients (including expansion and compression peaks) compare very well with the in-flight measurements.

This predicted behaviour is emphasized at M=1.052 (see FIG. 29) where in addition a stronger leeside shock wave, in front of the elevon, is predicted and also measured in flight. For this case, the comparison seems to be very good upstream of the elevon, both along wing leeside and windside.

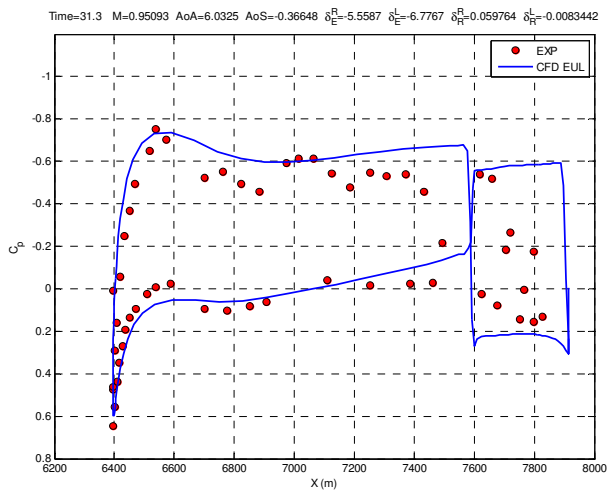

FIG. 28. Pressure coefficient at wing section y=1.0 m (M=0.951, α=6.03 deg, δ_E^R =-5.56 deg)

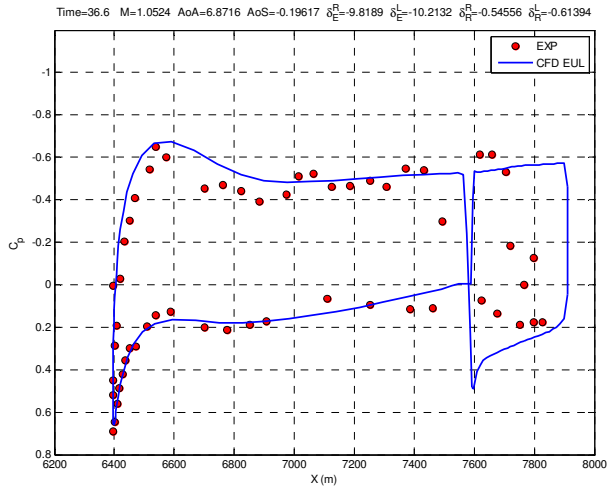

FIG. 29. Pressure coefficient at wing section y=1.0 m (M=1.052, α=6.87 deg, δ_E^R =-9.82 deg)

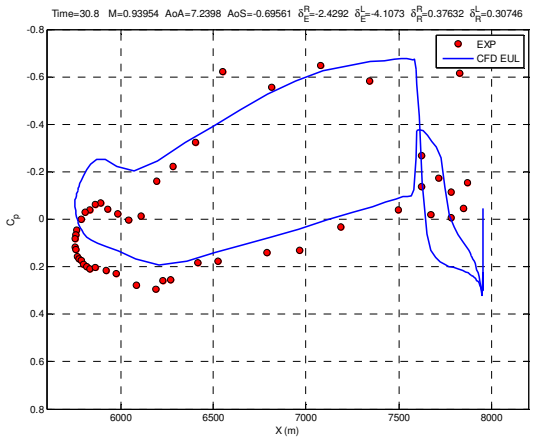

FIG. 30. Pressure coefficient at wing section y=0.65 m (M=0.94, α=7.24 deg, δ_E^R =-2.43 deg)

The comparison at the wing section y=0.65 m, located on the wing strake (see FIG. 30, M=0.940 condition) shows a shift between the CFD predicted and in-flight measured pressure coefficient distributions, especially around the wing leading edge, but a good similar trend. This discrepancy could be explained by a couple of reasons: first, the absence of viscous effects on CFD simulations as well and, second, the absence of such viscous effects on the local aerodynamic interference between the fuselage and the wing.

A very good comparison between CFD predictions and in-flight measurements can be observed also in FIG. 31, where the nose section at x=0.99 m is reported. The predicted pressure coefficient distribution at this section has been simply mirrored (computations have been performed on half vehicle), and the very good agreement justifies the hypothesis of assuming no sideslip (β=-0.36 deg in this flight condition) in the simulations, and is a further verification of the measured angle-of-attack. Note that one measurement on the fuselage upper part is clearly an outlier.

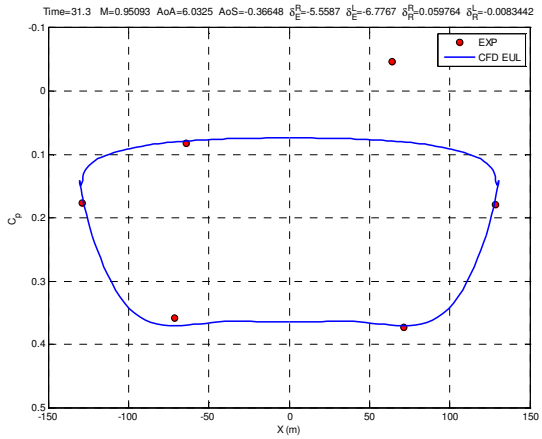

FIG. 31. Pressure coefficient at nose section x=0.99 m (M=0.951, α=6.03 deg, δ_E^R =-5.56 deg)

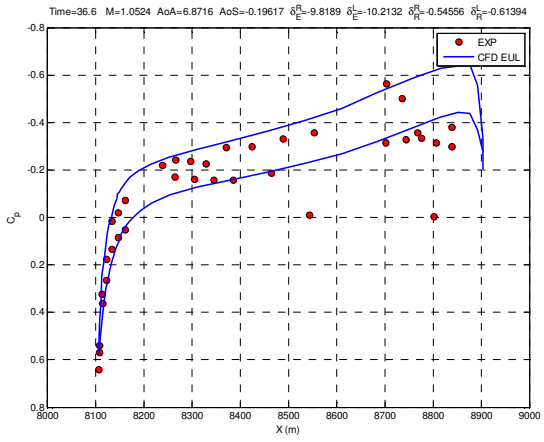

FIG. 32. Pressure coefficient along V-tail measurement line (M=1.052, α=6.87 deg, δ_E^R =-9.82 deg)

The comparison between CFD predicted and in-flight measured pressure coefficient along the vertical tail measurement line, at M=1.052, is reported in FIG. 32, and shows again a good agreement for the compression

peak at the leading edge and for a large part of the vertical tail, a small but not negligible side force generated by this control device (of course cancelled by the presence of the symmetric tail), and a small effect of the rudder deflection (δ_R^R =-0.55 deg in this flight condition).

8. CONCLUSIONS

Aim of this paper has been to show the preliminary results of the aerodynamic experiment performed during the first Dropped Transonic Flight Test of the Italian USV FTB-1 vehicle, mission flown on last February 24th, 2007 from the base of Arbatax in Sardinia, Italy. The main target of this experiment has been to provide a database of in-flight measurements of global (forces, moments) and local (static pressures) aerodynamic parameters useful to support and improve the CFD tools employed for the vehicle's design. As an overall goal of the USV project, this in-flight experimentation relies on the evaluation of the whole predictive capabilities and in its improvement finalized to design risk reduction.

Some selected flight conditions have been numerically rebuilt by means of Eulerian simulations, the attention being focused to the surface pressure distributions to be correlated with in-flight pressure measurements. The comparison between preliminary CFD Eulerian results and in-flight pressure measurements has shown that a good agreement has been achieved on the wing, especially on the levels of pressure coefficient along the leeside and the windside, including the expansion and the compression peaks downstream of the wing leading edge stagnation point. It is also evident how Eulerian computations do not predict the deterioration of pressure field on leeside due to the large separated area existing at relatively high angles of attack. The absence of viscous effects explain also some discrepancies on the pressure coefficient over the elevon, and on the not correctly predicted aerodynamic interference between the fuselage and the wing. The very good agreement between predictions and measurements on the front fuselage section justifies the hypothesis of assuming no sideslip in the simulations, and is a further verification of the measured angle-of-attack. The comparison is also good along the measurement line on the vertical tail.

As a rule of thumb, these CFD simulations have been finalised at reproducing the most relevant fluid dynamic phenomena characterizing the USV FTB-1 aerodynamics. The final objective of the present first DTFT mission post-flight analysis, currently on-going, is to carry out viscous fully turbulent or transitional simulations, to compare results to flight data and to improve and/or assess the entire CFD methodology, in terms of computational grids, turbulence and transition modelling, etc.

ACKNOWLEDGEMENTS

The authors are grateful to some CIRA people, in particular to Mr. Biagio Imperatore, Mr. Roberto Fauci and Mr. Michele Inverno for their precious help in selecting, implementing, verifying and acquiring the sensing equipment, and for having made exploitable the flight data; to Dr. Giuliano Ranuzzi for having developed and validated the H3NS code; and finally to the staff of the USV Program, mainly in the persons of Mr. Giuseppe Guidotti and the Program Manager Dr. Gennaro Russo.

REFERENCES

[1] Pastena M. et al., "PRORA USV1: The First Italian Experimental Vehicle to the Aerospaceplane", AIAA paper 2005-3406, *13th AIAA/CIRA International Space Planes and Hypersonic Systems and Technologies Conference*, Capua, Italy, May 16-20, 2005.

[2] Pamadi B.N. and Brauchmann G.J., "Aerodynamic Charact. and Development of the Aerodynamic Database of the X-34 RLV", Paper No. 17.1, *International Symposium on Atmospheric Reentry Vehicles and Systems*, Arcachon, France, March 16-18, 1999.

[3] Palazzo S. and Manco M., "CIRA USV Programme. Transonic Wind Tunnel Test Results on the USV FTB-1 Scaled Model in Longitudinal and Lateral-Directional Flight", CIRA-CF-04-0435, 2005.

[4] Gardner A.D. and Jacobs M., "Force and Moment Measurements on PRORA-USV 1:30 FTB1 Model in DNW-TWG June-July 2005", DNW IB 224-2005-C-11, August 2005.

[5] Gardner A.D. and Jacobs M., "Force and Moment Measurements on PRORA-USV 1:30 FTB1 Model in DNW-TWG January 2006", DNW IB 224-2006-C-24, January 2006.

[6] Roncioni P., Rufolo G.C., Votta R., Marini M., "An Extrapolation-To-Flight Methodology for Wind Tunnel Measurements Applied to the PRORA-USV FTB1 Vehicle", *International Astronautical Congress IAC2006*, Valencia, Spain, October 2-6, 2006.

[7] Votta R., Roncioni P., Rufolo G.C., Marini M., "A Preliminary CFD Analysis of the PRORA-USV Vehicle in Transonic and Low Supersonic Regime", EWHSFF-2005 Conference, Beijing, China, October 19-22, 2005.

[8] Andreutti G., "Studio delle derivate dinamiche latero-direzionali per il velivolo FTB1", CIRA-CF-04-0599, 2005.

[9] Mingione G. and Andreutti G., "Caratterizzazione aerodinamica del velivolo FTB1 in regime basso supersonico utilizzando metodologie semplificate", CIRA-CF-05-0633, October 2005.

[10] Rufolo G.C., Roncioni P., Marini M., Votta R., Palazzo S., "Experimental and Numerical Aerodynamic Data Integration and Aerodatabase Development for the PRORA-USV-FTB_1 Reusable Vehicle", AIAA paper 2006-8031, *14th AIAA/AHI International Space Planes and Hypersonic Systems and Technologies Conference*, Canberra, Australia, November 6-9, 2006.

[11] Cobleigh B.R., "Development of the X-33 Aerodynamic Uncertainty Model", NASA TP-1998-206544, April 1998.

[12] Ranuzzi G., Borreca S., "CLAE Project. H3NS: Code Development Verification and Validation", CIRA-CF-06-1017, 2006.